14th Australasian Fluid Mechanics Conference
Adelaide University, Adelaide, Australia
10-14 December 2001

A 3D Navier-Stokes Solver for the Design and Analysis of Turbomachinery

I. Huntsman[1] and R. Hothersall[2]

[1]Department of Mechanical Engineering
University of Canterbury, Christchurch, 8000, NEW ZEALAND

[2]CWF Hamilton and Co Ltd
Christchurch, 8000, NEW ZEALAND

Abstract

This paper presents the computational fluid dynamics (CFD) software developed at the University of Canterbury in conjunction with Hamilton Jet for the design of water jet impeller and stator components. The 3D software solves the Reynolds averaged Navier-Stokes equations on a finite volume "H" mesh. A second order upwind differencing scheme is used for the inviscid fluxes and the Baldwin-Lomax turbulence model is incorporated. A significant amount of research involved the validation of this software through experimental testing. Rotating and stationary blades of varying blade geometry, hub/casing ratio and profile were tested. The results of some of these tests are compared with the numerical predictions of the 3D program and are presented in this paper.

Introduction

Hamilton Jet and the University of Canterbury have an ongoing research and development programme which has involved the development of CFD capability for the hydrodynamic design of water jet impellers and stators. To minimise the number of prototypes required, the CFD software was specified as having to achieve design intent without having to resort to substantial experimental testing. The need to achieve design intent and a reduction in prototype testing required the CFD software to be able to differentiate between designs by resolving hydraulic losses (or entropy changes) and the modelling of three dimensional flow processes.

This paper presents comparisons between experimental measurements and predictions for a water jet impeller and, to demonstrate applicability to all types of turbomachine, a radial inflow turbine.

3D Flow Solver

The quasi-3-dimensional method used during the early parts of the design stage was previously described by Huntsman and Hodson[1]. There are several simplifying assumptions and empirical models to allow for the development of loss and blockage within the turbomachine. In order to gain confidence in any design prior to manufacture, or when trying many ideas to hone a design for optimal performance, a 3D method has been developed which uses fewer assumptions and empiricisms.

Numerical flow solvers are currently used to solve a wide variety of problems, covering the full speed range from low speed, incompressible flow to high speed, compressible flow.

In this work a "preconditioning" approach is used to permit solution of flows at any value of flow speed. This means that the resulting software may be used when solving water jet situations or for the flow of a compressible fluid (*e.g.* fans, compressors *etc*) without the need to develop a new method.

Governing Equations

The viscous flow of a Newtonian fluid is governed by the Navier-Stokes equations. The equations are presented below in integral, Cartesian form for an arbitrary control volume V with elemental surface area $d\boldsymbol{A}$:

$$\frac{\partial}{\partial t}\iiint \mathbf{W}dV + \iint (\mathbf{F}-\mathbf{D})\bullet d\mathbf{A} = \mathbf{0} \qquad (1)$$

where

$$\mathbf{W} = \begin{pmatrix} \rho \\ \rho v_x \\ \rho v_y \\ \rho v_z \\ \rho E \end{pmatrix},\ \mathbf{F} = \begin{pmatrix} \rho\mathbf{v} \\ \rho\mathbf{v}v_x + p\mathbf{i} \\ \rho\mathbf{v}v_y + p\mathbf{j} \\ \rho\mathbf{v}v_z + p\mathbf{k} \\ \rho\mathbf{v}E + p\mathbf{v} \end{pmatrix},\ \mathbf{D} = \begin{pmatrix} 0 \\ \tau_{xi} \\ \tau_{yi} \\ \tau_{zi} \\ \tau_{ij}v_j + \mathbf{q} \end{pmatrix}$$

and ρ, $\boldsymbol{v}$, E and p are the density, velocity, total energy per unit mass, and pressure of the fluid respectively. The term τ is the viscous stress tensor, $\boldsymbol{q}$ is the heat flux vector and $\boldsymbol{i}$, $\boldsymbol{j}$ and $\boldsymbol{k}$ are unit vectors in the Cartesian frame. $\mathbf{F}$ is the inviscid flux vector and $\mathbf{D}$ is the viscous flux vector.

When the solver is to be used with flows of variable density the Perfect gas law ($p = \rho RT$) is used as the equation of state. The term T is the fluid temperature. In the case of turbulent flows additional equations must be solved for turbulence closure. In the present work the algorithm and technique will be demonstrated for flows which use the Baldwin-Lomax[2] model for turbulent closure.

Preconditioning

In their original form time-marching schemes were not able to solve low speed or incompressible flow because the continuity equation becomes uncoupled from the momentum and energy equations. The artificial compressibility approach of Chorin[3] and Rogers and Kwak[4] introduces a pressure term into the continuity equation. The pressure term is normalised by a pseudo-acoustic speed. The pseudo-acoustic speed may be set to any value and methods for its determination are suggested by several authors, Rogers and Kwak[4] and Weiss and Smith[5]. The use of a pseudo-acoustic speed makes the governing equations hyperbolic but removes the time accuracy of the method. Time accurate results may still be obtained if the algorithm is developed in a slightly different manner (Chorin[3] and Weiss and Smith[5]).

In the preconditioning technique the Navier-Stokes equations are re-written in terms of the primitive variables $\mathbf{Q} = [\ p,\ v_x,\ v_y,\ v_z,\ T]^T$ as (Weiss and Smith[5]):

$$\mathbf{K}\frac{\partial \mathbf{W}}{\partial \mathbf{Q}}\frac{\partial}{\partial t}\iiint \mathbf{Q}dV + \iint (\mathbf{F}-\mathbf{D})\bullet d\mathbf{A} = \mathbf{0} \qquad (2)$$

where K is the preconditoning matrix and $\partial\mathbf{W}/\partial\mathbf{Q}$ is the Jacobian of the conservative and primitive variables. The preconditioning matrix and the Jacobian may be combined to form the matrix

$\Gamma = \mathbf{K}\,\partial\mathbf{W}/\partial\mathbf{Q}$:

$$\Gamma = \begin{pmatrix} \Theta & 0 & 0 & 0 & \rho_T \\ \Theta v_x & \rho & 0 & 0 & \rho_T v_x \\ \Theta v_y & 0 & \rho & 0 & \rho_T v_y \\ \Theta v_z & 0 & 0 & \rho & \rho_T v_z \\ \Theta h_0 - \delta & \rho v_x & \rho v_y & \rho v_z & \rho_T h_0 + \rho c_p \end{pmatrix} \quad (3)$$

where ρ_T is the derivative of density with respect to temperature at constant pressure and h_0 is the stagnation enthalpy. The value of ρ_T is zero in incompressible flow. For incompressible flow $\delta = 0$, whereas for compressible flow $\delta = 1$. The parameter Θ is defined as:

$$\Theta = 1/U_r^2 - \rho_T/\rho c_p \quad (4)$$

The reference velocity U_r in equation (4) is chosen so as to maintain well conditioned eigenvalues for the system. For low speed and incompressible flow either the local velocity or a pseudo-acoustic velocity may be specified. In the present work both methods were found to give satisfactory results but the rate of convergence was significantly increased by using a pseudo-acoustic speed based on the average of the velocities at the inlet and outlet to the solution domain, $\overline{|V_{in/out}|}$. As the speed of the flow increases, the reference velocity is limited to be no greater than the local sonic speed, c, as this maintains the correct transonic and supersonic behaviour.

Discretisation of the preconditioned Navier-Stokes equations in space transforms the governing equations into a set of coupled ordinary differential equations that must be integrated in time to obtain the steady state solution. In this work, an explicit scheme has been chosen for simplicity and four levels of multi-grid have been used to accelerate convergence. Integration to a steady state is performed by using a five stage hybrid Runge-Kutta scheme.

The dissipation terms are only evaluated at the first stage of the integration as this is a particularly computationally intensive step. The overall convergence of the method was observed to occur in a shorter time when this simplification was made. The inviscid fluxes **F**(Q) have been evaluated using an upwind, flux difference splitting approach. The method chosen is the approximate Reimann solver due to Roe[6], with a variable extrapolation, MUSCL approach (van Leer[7]) to increase accuracy to second order. The second order numerical scheme is not generally stable so the gradients used in the MUSCL approach have been limited using the method due to van Albada *et al*[8]. The time-step size varies locally to maintain a CFL number of between 1 and 2 at each cell.

At the inlet boundary the flow direction and either the mass flow rate or the stagnation values of pressure and temperature are fixed. At the outlet the hub pressure is fixed and the variation of pressure with radius is determined from radial equilibrium. At the solid boundaries either the law of the wall or a laminar no-slip boundary condition are used to determine the local shear stress, depending upon the local Reynolds number.

Experimental Arrangement

Experimental data will be presented from two test rigs. Water jet testing of impellers and stators is carried out in the Hamilton Jet test rig. The rig is a closed circuit arrangement, in which the pressure may be adjusted. Flow straighteners and settling lengths are employed to ensure uniform flow upstream of the impeller and upstream of the orifice. The water temperature is monitored and held to around 15°C.

A BS1042 orifice is used to measure flow rate via a differential pressure transducer and piezometer rings. The pressure rise across the pump is measured by a differential pressure transducer and piezometer rings at stations upstream and downstream from the water jet. The power absorbed is obtained from a torque transducer and rotational speed data. There are measurement planes upstream of the rotor, between the rotor and the stator and downstream from the stator. A 3-hole probe may be traversed across any of the measurement planes. A three hole probe is satisfactory only when the radial velocity components are negligible. Traverses between the stator and impeller were carried out using a hub spacer which allowed the flow to become predominantly axial in nature.

The radial turbine used for the present investigation was designed to be representative of current design philosophies for radial inflow turbines and has been described by Huntsman *et al*[9]. The turbine is the low-speed aerodynamic model of a radial turbine designed by Rolls-Royce as the gas generator for a helicopter engine. The meridional geometry and blade profiles of the model turbine were varied to compensate for the density change in the high-speed turbine. The rig operates as an open loop wind tunnel drawing air from the atmosphere through an axisymmetric bellmouth into the turbine. A filter surrounds the bellmouth. A volute is not used in this machine but there are 23 radial flow stator blades which deflect the air through an angle of 71°. The flow enters the rotor at an angle in the relative frame of -19°. The air leaves the rotor predominantly in the axial direction and travels along a circular exhaust duct through a honeycomb flow straightener to a sliding, axisymmetric throttle and the suction fan. At the rotor exit, there is a rotating *radial-circumferential* traverse system which enables the acquisition of data from the rotating frame of reference. Sliprings were used to carry the control and monitoring signals to the traverse system. Area traversing has been undertaken in the relative and stationary frames of reference using a fixed-direction 5-hole pyramidal pneumatic probe. This was calibrated for the measurement of yaw and pitch angles, total pressure and dynamic head.

The flow visualisation technique described by Joslyn and Dring[10] has been used for the surfaces of the rotor blades. This technique uses ammonia gas and "Ozalid" paper. The paper was stuck onto the surface of the rotor blade which was instrumented with pressure tappings. Small holes were punched through the paper adjacent to the pressure tappings. With the rig running at the desired operating point, ammonia gas was ejected at low speed from the tappings. Where the ammonia gas comes into contact with the Ozalid paper a chemical reaction occurs to change the colour of the paper from white to black. The black marks extending from the tapping indicate the flow direction of the ammonia close to the surface.

Results and Discussion

A number of water jet impeller designs have been tested including a 5 blade "production" HJ 321 impeller. A perspex impeller housing and a standard production stator were used.

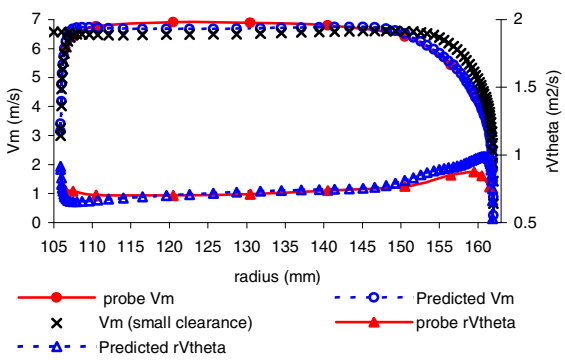

Figure 1. v_m, rv_θ plotted against radius for the HJ 321 impeller

Experimental measurements of meridional velocity, v_m, radius multiplied by swirl velocity, rv_θ, absolute flow angle (yaw) and relative flow angle (beta) are plotted (solid lines and solid

circles/triangles) in Figures 1 and 2. The probe was located about one blade span downstream of the impeller.

The 3D solver output, presented as a mass weighted pitchwise average for v_m, rv_θ, yaw and beta, matches the probe data closely as seen in Figures 1 and 2. Yaw is predicted within about 1° and relative flow angle within ½°. The blade angles are shown to indicate the amount of deviation present, and to reinforce the accuracy of the prediction. The 3D solver meridional velocity distribution, v_m, matches well with the measured distribution except in the hub region.

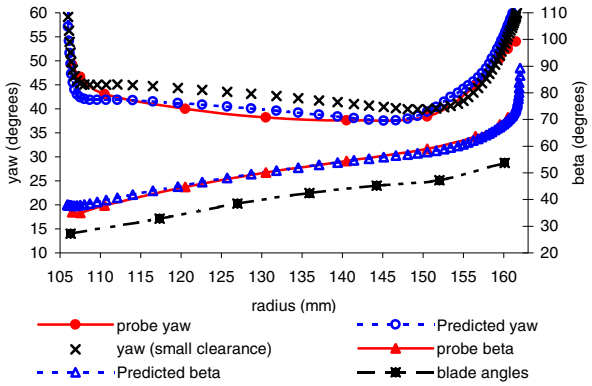

Figure 2. yaw and beta plotted against radius for the HJ 321 impeller

The ability to predict impeller power absorption is a key application requirement. The v_m and rv_θ distribution from the 3D solver output in Figure 1 can be integrated to obtain an impeller rating. This corresponds to 24.3 kW with casing shear work component accounted for. The torque and rpm data measured directly on the test rig, with bearing friction subtracted, yield an impeller rating of 23.9 kW. The predicted output produces an impeller rating which is about 1.6% too high.

The key to successful hydrodynamic design of fluid machinery is in understanding the causes of different types of hydraulic loss, predicting their magnitudes and developing ways to minimise them. The 3D solver will make a reasonable attempt at predicting the magnitude of the hydraulic losses. More important though is the ability to show relative changes for different design solutions. Flow near the casing is dominated by the tip clearance flow. This results in both a significant blockage effect and a loss. The significance of this is seen by the 3D solver output for a smaller tip clearance. The data shows an increase in v_m at the tip and a reduction in v_m across the bulk of the blade span. The relative flow angle remains unchanged but a dramatic change in yaw angle of the order of 3° occurs. The change in the velocity distribution and the yaw angle has a large affect on the power absorbed by the impeller. With the tip clearance halved the impeller rating changes to a value about 7% too high

The radial turbine facility has the ability to obtain rotating frame area traverse data so the development of the losses in the turbine may be measured. The 5-hole pneumatic probe was traversed in both the circumferential and radial directions just upstream of the trailing edge of the rotor. The boundary layers on the surfaces of the rotor blades were not measured. The diameter of the 5-hole probe was 2mm and the pitch of the blades at the mid-span is 140mm. The coefficient for the loss of stagnation pressure has been calculated from the measurements at the rotor exit and is shown in figure 3 for the design flow condition. There is little deficit of stagnation pressure in the flow away from the blade surface boundary layers. Near the casing, however, there are two distinct high loss regions. Huntsman and Hodson[11] reported the origin of the different loss regions previously.

The region of high loss of stagnation pressure near the casing of figure 3 is due to the entropy creation within the clearance vortex. The large extent of loss at about 80% span is largely due to the accumulation of low momentum fluid from the casing endwall (the "scraping" vortex). The flow induced near the suction surface by the scraping vortex is towards the hub and will be discussed further later.

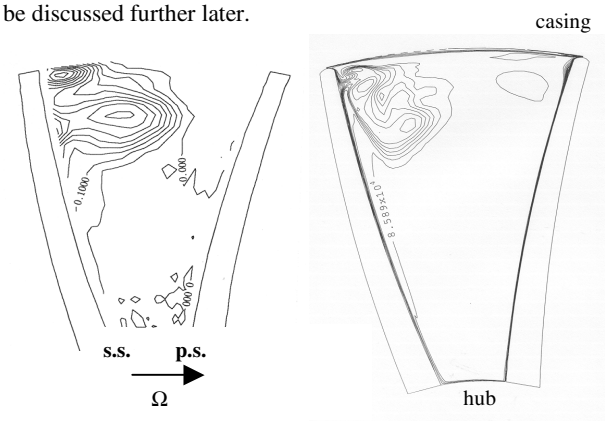

(a) Measured (b) Predicted

Figure 3. Measured and predicted pressure loss contours near the trailing edge of the radial inflow turbine.

There is another contribution to the lower part of the large loss region due to the accumulation of the secondary flow on the suction surface near the casing. The secondary flow moved under the influence of the gradient of reduced static pressure on the suction surface towards the minimum pressure at the casing.

The largest feature observed in this turbine is the scraping vortex. The tendency to form a scraping vortex is present in all radial inflow turbines. The predictions shown in figure 3 show the same general features and that the sizes of each loss region are similar. This is the reason why the pitchwise averaged data shown earlier are similar between prediction and experiment.

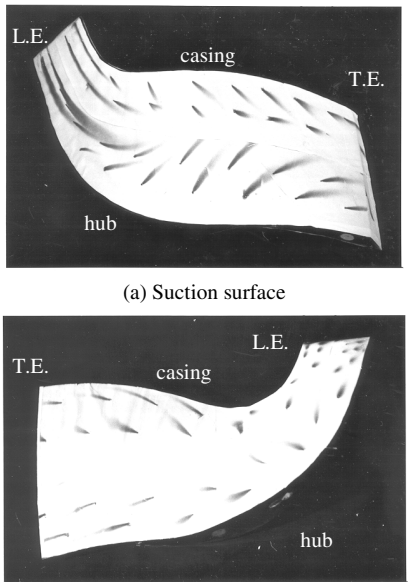

(a) Suction surface

(b) Pressure surface

Figure 4. Flow visualisation at an incidence angle of -27°

Figure 4 presents the flow visualisation at the flow condition that corresponds to an incidence angle of -27° at the inlet to the rotor. The flow visualisation on the pressure surface shows that there is a large region of reversed flow up to 20% surface length. This is due to separation of the boundary layer from the blade surface. The boundary layer is unable to withstand the adverse pressure gradient which occurs during the deceleration after the large

overspeed at negative incidence. This large separation bubble is likely to be present in all radial turbines when operating at relatively small amounts of negative incidence because nearly all radial turbines have radial blades at the rotor inlet. Figure 4 shows that close to the downstream end of the large separation bubble the low momentum fluid moves towards the casing under the influence of the pressure field generated by the meridional curvature. Near the leading edge the low momentum fluid moves towards the hub as a result of the blade lean. On the suction surface, the flow near the leading edge does not separate. Near the casing, in the exducer, on the pressure surface, the flow close to the blade surface, has a component of velocity towards the casing. In the same region of the blade, on the suction surface, the secondary flow moves towards the hub.

Figure 5 shows the predicted velocity vectors close to the blade surfaces. Comparison between figures 4 and 5 show that the effects of the scraping vortex are well resolved and that the separation bubble at the leading edge of the pressure surface is well predicted. The secondary flow within the separation bubble is also well resolved.

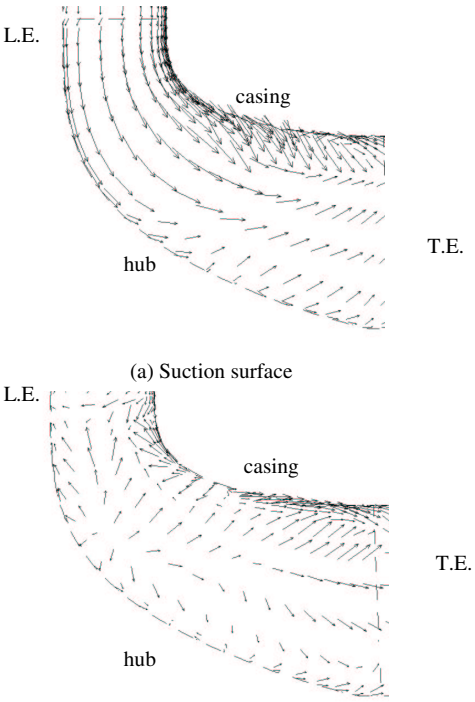

(a) Suction surface

(b) Pressure surface

Figure 5. Predicted velocity vectors close to the blade surfaces.

Figure 6 shows the variation of the coefficient for the loss of stagnation pressure for the flow condition which corresponds to an incidence angle of -27°. The regions of high loss occupy a large proportion of the span. The effect of the small clearance vortex is barely noticeable. At negative incidence there is increased shear at the casing and reduced blade loading relative to the design flow condition (for the same Reynolds number). Consequently, there is reduced mass flow through the clearance gap and a smaller clearance vortex.

At 80% span the accumulation of the secondary flow due to the "scraping" effect at the endwall may be observed. The third high loss region near to the mid-span position on figure 6 was not present in the other data that has been presented. The sign of the secondary vorticity associated with this region is positive. Consequently, it is believed that this region on the figures is due to the accumulation of the secondary flow on the suction surface. The predicted variation of stagnation pressure loss shows the same features as the measured data, although there is a slight variation in the size and location of the features. Generally the prediction of this complex off-design flow condition is well resolved.

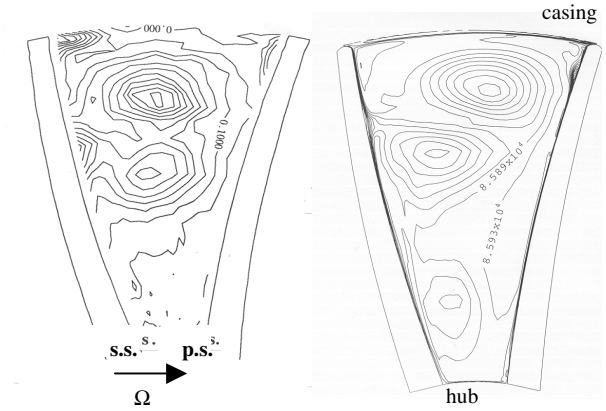

(a) measured (b) predicted

Figure 6. Measured and predicted pressure loss contours near the trailing edge of the radial inflow turbine at an incidence angle of -27°.

Further analysis of the stagnation pressure losses reveal that the change in efficiency between the design condition and the negative incidence condition corresponds to about 7%. The predicted variation in efficiency is just over 6% showing good agreement between prediction and experiment.

Conclusions

A 3D flow solver has been presented. The predictions from the solver have been shown to agree well with data from a waterjet impeller and the rotor of a radial inflow turbine.

Acknowledgments

This work was performed with financial assistance from the New Zealand Foundation for Science Research and Technology, TBG grant number HAM501.

References

[1] Huntsman, I. and Hodson, H. P., "Measurements and predictions of the flow around the leading edge of a radial inflow turbine rotor", Tenth International Symposium on Air Breathing Engines, Vol. 1, pp. 431-438, 1991

[2] Baldwin, B. and Lomax, H., "Thin layer approximation and algebraic model for separated turbulent flows", AIAA paper, 78-257, 1978

[3] Chorin, A.J., "A numerical method for solving incompressible viscous flow problems", *Journal of Computational Physics*, vol 2, no 1, pp. 12-16, 1967

[4] Rogers, S.E. and Kwak, D., "Upwind differencing scheme for the time accurate incompressible Navier-Stokes Equations", *AIAA Journal*, vol 28, no 2, pp. 253-262, 1990

[5] Weiss, J.M. and Smith, W.A., "Preconditioning applied to variable and constant density flows", *AIAA Journal*, vol 33, no 11, pp. 2050-2057, 1995

[6] Roe, P.L., "Characteristic based schemes for the Euler equations", *Annual Review of Fluid Mechanics*, vol 18, pp. 337-365, 1986

[7] van Leer, B., "Towards the ultimate conservative difference. V. A second order sequel to Godunov's method", *Journal of Computational Physics*, 32, pp. 101-136, 1979

[8] van Albada, G. D., van Leer, B. and Roberts, W. W., "A comparative study of computational methods in cosmic gas dynamics", *Astron. Astrophysics*, **108**, pp. 76-84, 1982

[9] Huntsman, I., Hodson, H.P. and Hill, S.H., "The design and testing of a radial flow turbine for aerodynamic research", *Journal of Turbomachinery*, Vol. 114, pp. 411-418, 1992

[10] Joslyn, H. D. and Dring, R. P., 1983, "Turbine rotor negative incidence stall", ASME paper no. 83-GT-23

[11] Huntsman, I. and Hodson, H.P., "An experimental assessment of the aerodynamic performance of a low-speed radial inflow turbine", AIAA paper 94-2932, 1994